https://doi.org/10.1016/j.geothermics.2018.06.008

Thermodynamic Analysis of a Power and Water Combined System with Geothermal Energy Utilization

W.F. He[1,2*], H.X. Yang[1], D. Han[2]

1. Renewable Energy Research Group, Department of Building and Service Engineering, The Hong Kong Polytechnic University, Hong Kong, China

2. College of Energy and Power Engineering, Nanjing University of Aeronautics and Astronautics, Nanjing, China

Corresponding author: W.F. He

The Hong Kong Polytechnic University, Hung Hom, Kowloon, Hong Kong, China

E-mail address: wfenghe@polyu.edu.hk, wfhe@nuaa.edu.cn

ABSTRACT: A novel combined system, integrated with a flashing Ranking cycle and humidification dehumidification (HDH) desalination unit, is proposed to achieve the energy utilization from geothermal water. The flashed steam is used to generate power while the remaining water is applied to heat the seawater for water production. Based on the coupling relation between the power and desalination unit, conservation equations based on the thermodynamic laws are constituted. Energy and entropy analysis of the combined system are achieved for determining the power and water production. Furthermore, the influence principles from the spraying temperature and terminal temperature difference of the seawater heater on the overall performance of the combined system are also focused. The simulation results indicate that the maximal net power from the flashing Rankine cycle reaches 157.0kW when the flashing temperature is 375.15K. Due to the leading role to determine total efficiency of the combined system, maximum values of 711.85kgh^{-1} for the water production and 43.98% for the total efficiency are obtained when the flashing temperature is 378.15K. Furthermore , it is also obtained that a lower value both for the seawater spraying temperature and terminal temperature difference of the seawater heater can help to improve the performance of the combined system.

Keywords: flashing Rankine cycle; humidification dehumidification; desalination; geothermal water; total efficiency

Nomenclature

Roman symbols

h	enthalpy ($kJkg^{-1}$)
h_{fg}	latent heat ($kJkg^{-1}$)
L	length along the heat exchanger (mm)
m	mass flow rate (kgs^{-1})
p	pressure (MPa); wet perimeter (m)
Q	heat load (kW)
RH	relative humidity
s	specific entropy ($kJkg^{-1}K^{-1}$);
S	concentration of seawater (gkg^{-1}); entropy rate ($kJs^{-1}K^{-1}$)
T	temperature (K)
W	power (kW)
Greek letters	
ε	effectiveness of the humidifier and dehumidifier
ρ	density (kgm^3)
η	efficiency
ω	humidity ratio (gkg^{-1})
Subscripts	
a	air
b	brine
c	condenser
d	dehumidifier
da	dry air
e	exhaust
FE	flashing evaporator
fs	flashed steam
fw	flashed water
gen	generation
gw	geothermal water
h	humidifier
i	inlet
m	maximum
o	outlet
p	pump
SH	seawater heater
sw	seawater

t	total
tur	turbine
v	valve
w	water

1. Introduction

In view of the unsustainable development in the past centuries, the crisis of energy and freshwater are becoming a reality gradually. As a result, energy and water supply with clean and efficient method has attracted more and more attentions. Thereinto, geothermal resources, which mainly contain geothermal dry steam, geothermal wet steam and geothermal water belongs to the renewable energy, and they are first applied investigated and applied to achieve the power generation all over the world [1, 2].

Jalilinasrabady [3] first designed a single flash cycle for power generation with geothermal energy, which has a temperature of 513K. Based on the developed mathematical models for thermodynamic analysis, it was found that the proposed scheme can obtain a maximum net power output, 31 MW, when the flashing and discharged pressures were fixed at 5.5 bar and 0.3 bar, respectively. For the sake of a optimized energy utilization, a double flash configuration was then advised, and the relevant maximum net power can arrive at 49.7 MW. In combination with the exergy analysis, a double flash cycle system for the Sabalan power plant was finally proposed. Yari [4] achieved a comparative investigation for different types of geothermal power plant, aiming to high temperature geothermal resources with a temperature of 503K. Mathematical models for each contained thermal cycle was developed, with model validation by previous published data. After the energy and exergy analysis, the results comparison was completed for clarifying the best cycle configurations. It was found that the thermal efficiency of the binary cycle with a regenerative ORC have the highest efficiency of 15.35%. Wang [5] introduced a Kalina cycle for further heat recovery of geothermal water from a primary flashing cycle, powered by the geothermal water with a temperature of 443K. Based on the established mathematical models of the flash-binary geothermal power generation system, the influences from critical thermal parameters are examined, and an optimization

method was also proposed to determine the best performance with exergy efficiency as the objective function. It was discovered that the best exergy efficiency of the system can arrive at 37.01% under the prescribed input boundaries. Yang [6] proposed an organic Rankine cycle to generate power with geothermal resource from abandoned oil wells, with a temperature of 383K. With R245fa as the cycling working fluid, a four-stage axial turbine was appointed in the ORC, and an onsite test showed that the efficiency of the turbine and entire cycle can reach 78.52% and 5.33%, respectively. The research results and method could give some significant references for the desirable power plants with the geothermal energy from the abandoned oil wells.

Based on the aforementioned literature, it can be concluded that the configurations of the power system should be determined by the temperature and components of the geothermal resources [7, 8]. For a high temperature geothermal resource, the flashing cycle and low temperature power cycles [9-11] are always existing simultaneously for the sake of energy cascade utilization. However, in most occasions, power and water are both in rigid demand to satisfy the industrial production and life. Accordingly, in the binary power systems powered by geothermal energy, searching an appropriate desalination method to replace the low temperature power cycle to recover the carried heat of the water from the primary flashing section for water production can achieve the problem. Recent years, the humidification dehumidification methods [12, 13], which has the great advantages, has been one of the major research focus in the field of desalination.

A saturated air cycling within the HDH desalination unit was assumed to investigate the relevant system performance by Campos [14]. Through the experimental test, the internal parameters were selected to minimize the residual summation of the contained temperature values. Based on the validated the mathematical models, a sensitive analysis from critical parameters on the water production capacity was completed. From the test results, it was observed that the heat load of the solar heater, humidifier height and seawater mass flow rate were the most critical impact factors to change the production, while the influences from the ambient temperature was very slight.

Dual solar collectors to heat water and air simultaneously were applied in a HDH desalination system by Rajaseenivasan [15], and the relevant experimental platform was built. After the test, it was found that the mass flow rate and operation temperatures of the working fluid were related to the water producing capacity. An overall efficiency of the system with the concave turbulators arrived at 67.6%. At the aspect of the water production, the highest values reached 12.36, 14.14 and 15.23 kgm^{-2} one day for the schemes without turbulators, convex and concave turbulators, respectively. Siddiqui [16] studied the performance of an HDH desalination system operated under vacuum environment. Based on the established mathematical models, it was found that the gain output ratio would be raised after decreasing the humidification pressure. Kabeel [17] tested the performance of a HDH system incorporated by an indirect solar dryer. It was discovered that the gain output ratio of the modified system was enlarged by 29%, and it was raised with increasing the air flow rate. In addition of the solar energy, geothermal energy was also used to power the HDH desalination unit by Mohamed [18] and Elminshawy [19]. After the integration between the geothermal resource and HDH desalination unit, the relevant performance was investigated by theoretical and experimental analysis, respectively. In spite of the different effect in each system, the common viewpoint was gained that only the low temperature geothermal resource was suitable for the desalination system.

Due to the absence of the integration between the flashing Rankine cycle and the HDH desalination unit, the present paper focuses on the performance of such combined system for power and water joint production. Based on the thermodynamic laws, the mathematical models of the combined system were built, and then the corresponding energy and entropy analysis for the subsystems and entire system were completed. Furthermore, the influences from the seawater spraying temperature and terminal temperature difference of the seawater heater are also studied. The research results provide significant references for the innovative design and further optimization of the power and water combined systems.

2. System description

The detailed scheme of the novel power and water system, with flashing Rankine cycle and HDH desalination cycle coupled, is exhibited in Fig. 1. Obviously, the power and water supply system consist of the flashing Rankine cycle and HDH desalination cycle. For the aspect of the flashing Rankine cycle, the geothermal water is first pressurized in the pump, and then flows into the flashing evaporator. After the sudden pressure declination, saturated steam is obtained, and then the flashed steam flows into the steam turbine. During the expansion of the steam, output power is obtained from the generator. Finally, the discharged steam from the turbine is condensed under the cooling effect of the ambient seawater, with the temperature profile in Fig. 2 (a), and the condensate become part of the backflow for the geothermal water.

At the bottom of the flashing evaporator, the hot flashed water enters the seawater heater to raised the temperature of the preheated seawater from the dehumidifier, with the temperature profile shown in Fig. 2 (b). The hot seawater is sprayed into the humidifier packings in the nozzles, and contact the humid air direct. As a result, the temperature as well as the humidity ratio of the air is elevated, with the Psychrometric chart in Fig. 2 (c), transferring heat and mass with the seawater, while the seawater is concentrated with the brine flowing out of the humidifier. Afterwards, the hot humid air flows into the dehumidifier, and it is condensed while the ambient seawater is preheated outside. Finally, due to the decrease of the humidity ratio for the humid air, freshwater is gained at the bottom of the dehumidifier. With respect to the flashed geothermal water, it is cooled after the temperature of the seawater is raised, and then it is throttled in the valve for an equilibrium pressure with the condensate from the condenser. It can be concluded that the geothermal water is applied to drive the power plant and HDH desalination system successively, and the discharged water flows back into the geothermal well finally.

For the sake of the mathematical models for the power and water combined system, assumptions are given out to achieve the investigation successfully as follows:

(1) Both the flashing Rankine cycle and HDH desalination cycle run at steady-state conditions.

(2) Energy loss to the environment, changes of the potential and kinetic energy within the heat exchangers are neglected.

(3) Fouling thermal resistance of the heat exchangers is not considered.

(4) Flow loss within the heat exchangers and pipes in the entire combined system is ignored.

3. Mathematical models

3.1 Flashing Rankine cycle

Water Pump

In order to utilize the geothermal water, a pump should be first installed to drive the water flow into the flashing evaporator, and the consumed power can be calculated in Eq. (1) with η_p=0.75.

$$W_p = \frac{m_{gw}}{\rho_{gw}\eta_p}(\Delta p_{FE} + \Delta p_v) = \frac{m_{gw}(h_{gw,p} - h_{gw,i})}{\eta_p} \quad (1)$$

where m_{gw} and ρ_{gw} are the mass flow rate and density of the inflow geothermal water, Δp_{FE} and Δp_v the pressure drop in the flashing evaporator and value, and $h_{gw,i}$ and $h_{gw,p}$ are the specific enthalpy of the geothermal water at the inlet and outlet of the pump. Besides the energetic analysis for the thermal process, the entropy analysis should also be executed to inspect the corresponding feasibility and irreversible loss. Hence, the entropy generation rate during the pump process, $S_{gen,\,p}$, can be expressed as follows:

$$S_{gen,p} = m_{gw}(s_{gw,p} - s_{gw,i}) \quad (2)$$

where $s_{gw,i}$ and $s_{gw,p}$ are the specific entropy of the geothermal water at the inlet and outlet of the pump.

Flashing Evaporator

In order to obtain the steam from power generation, the geothermal water must first be flashed in the evaporator. According to the theory of thermodynamics, flashing process of the water will occur when the pressure suddenly drops, and then the saturated steam and water at a lower pressure will be attained. Obviously, according to the mass and energy balance during the flashing, the conservation equations, including the mass, energy and

entropy, can be listed as follows:

$$m_{gw} = m_{fs} + m_{fw} \tag{3}$$

$$m_{gw} h_{gw,p} = m_{fs} h_{fs} + m_{fw} h_{fw} \tag{4}$$

$$S_{gen,FE} = m_{fw} s_{fw} + m_{fs} s_{fs} - m_{gw} s_{gw,p} \tag{5}$$

where m_{fs} and m_{fw} are the mass flow rates of the flashed steam and water, h_{fs} and h_{fw} are the specific enthalpy of the flashed steam and water, respectively, s_{fw} and s_{fs} the specific entropy of the flashed water, flashed steam.

Steam Turbine

The saturated steam from the top of the flashing evaporator flows into the steam turbine, and the output power obtained from the generator can be calculated at the fixed value for η_{tur}=0.8 in Eq. (6).

$$W_{tur} = m_{fs}(h_{fs} - h_{es})\eta_{tur} \tag{6}$$

where h_{es} is the specific enthalpy of the discharged steam during an isentropic expansion. For the entropy analysis, the entropy generation rate during the expansion can be calculated in Eq. (7).

$$S_{gen,tur} = m_{fs}(s_e - s_{fs}) \tag{7}$$

where s_e is the specific entropy of the discharged steam out of the turbine. Hence, after the acquisition of the output power from the turbine and the consumed power of the pump, the final net power can be calculated in Eq. (8) with η_m=η_g=0.98.

$$W_{net} = W_{tur}\eta_m\eta_g - W_p \tag{8}$$

Condenser

After the expansion process, the discharged steam from the turbine enters the condenser, and it is cooled and condensed under the cooling effect of the ambient seawater. Consequently, the energy and entropy balance within the condenser can be expressed as:

$$Q_c = m_{fs}(h_e - h_c) = m_c(h_{sw,o} - h_{sw,i}) \tag{9}$$

$$S_{gen,c} = m_c(s_{sw,o} - s_{sw,i}) + m_{fs}(s_c - s_e) \quad (10)$$

where h_e and h_c represent the specific enthalpy of the discharged steam and the condensate, m_c the mass flow rate of the cooling seawater, $h_{sw,i}$ and $h_{sw,o}$ the corresponding specific enthalpy at the condenser inlet and outlet [20], $s_{sw,i}$ and $s_{sw,o}$ the corresponding specific entropy of the seawater, s_c the specific entropy of the condensate.

3.2 HDH desalination cycle

Seawater Heater

For the HDH desalination cycle, it is driven by the flashed water from the bottom of the flashing evaporator. Accordingly, the temperature of the seawater is elevated to a top value in the seawater heater, and the relevant heat transfer load can be calculated in Eq. (11).

$$Q_{SH} = m_{fw}(h_{fw} - h_{SH}) = m_{sw}(h_{sw2} - h_{sw1}) \quad (11)$$

where h_{SH} is the specific enthalpy of the flashed water at the outlet of the seawater heater, m_{sw} the mass flow rate of the involved seawater, h_{sw1} and h_{sw2} the corresponding specific enthalpy at the heater inlet and outlet. In addition of the heat load of the heater, the relevant entropy balance can also be described as:

$$S_{gen,SH} = m_{fw}(s_{SH} - s_{fw}) + m_{sw}(s_{sw2} - s_{sw1}) \quad (12)$$

where s_{SH} is the specific entropy of the flashed water at the outlet of the heater, while s_{sw1} and s_{sw2} are the specific entropy before and after the heating process.

Packed Bed Humidifier

In order to elevate the temperature and humidity ratio of the air for water production, packed bed is applied in the humidifier. Hence, the sprayed seawater and humid air contact direct, and heat and mass transferring processes arise simultaneously. During the humidification, the corresponding mass and energy balance can be described as:

$$m_{sw} - m_b = m_{da}(\omega_2 - \omega_1) \quad (13)$$

$$m_{sw}h_{sw2} - m_b h_b = m_{da}(h_{a2} - h_{a1}) \quad (14)$$

where m_b is the mass flow rate of the concentrated brine while m_{da} is the mass flow rate of the dry air, ω_1 and ω_2 the air humidity ratio at the inlet and outlet of the humidifier, h_{sw2} and h_b the specific enthalpy of the sprayed seawater and brine, h_{a1} and h_{a2} the specific enthalpy of the humid air at the inlet and outlet, respectively [21]. With respect to the entropy equation, the entropy generation rate within the humidifier, $S_{gen,h}$, can be acquired.

$$S_{gen,h} = m_b s_b - m_{sw} s_{sw2} + m_{da}(s_{a2} - s_{a1}) \tag{15}$$

where s_b represents the specific entropy of the hot brine at the bottom of the humidifier, while s_{a1} and s_{a2} are the specific entropy of the humid air before and after humidification.

Dehumidifier

After the humidification is completed, a heat exchanger is used to cool the hot humid air, and hence fresh water can be gained during the dehumidification. Consequently, the relevant conservation equations can be acquired.

$$m_w = m_{da}(\omega_2 - \omega_1) \tag{16}$$

$$m_{sw}(h_{sw1} - h_{sw,i}) = m_{da}(h_{a2} - h_{a1}) - m_w h_w \tag{17}$$

where m_w and h_w are the mass flow rate and specific enthalpy of the produced water from the dehumidified heat exchanger. Additionally, the corresponding entropy generation rate, $S_{gen,d}$ during the dehumidification can be acquired in Eq. (18).

$$S_{gen,d} = m_{sw}(s_{sw1} - s_{sw,i}) + m_{da}(s_{a1} - s_{a2}) + m_w s_w \tag{18}$$

where s_w stands for the specific entropy of the produced fresh water.

Valve

In order to discharge the cooled flashed water, the flashed water out of the seawater heater should be first throttled within the valve. The expression of isenthalpic process can be expressed as:

$$h_{SH} = h_v \tag{19}$$

where h_v is the specific enthalpy of the flashed water at the outlet of the valve. Furthermore, the entropy generation rate during the isenthalpic process can also be obtained.

$$S_{gen,v} = m_{fw}(s_v - s_{SH}) \tag{20}$$

where s_v stands for the specific entropy of the flashed water at the outlet of the valve.

Mixer

Afterwards, the throttled water joins the condensed water from the flashing Rankine cycle. Hence, the final cooled geothermal water can be obtained, and the relevant mass and energy balance during the mixing process can be expressed in Eq. (21) and Eq. (22).

$$m_{fw} + m_{fs} = m_{gw} \tag{21}$$

$$m_{fw}h_v + m_{fs}h_c = m_{gw}h_{gw,o} \tag{22}$$

where $h_{gw,o}$ is the specific enthalpy of the final geothermal water into the well, and the entropy generation rate during the mixing between the condensate and the flashed water can be obtained.

$$S_{gen,m} = m_{gw}s_{gw,o} - m_{fw}s_v - m_{fs}s_c \tag{23}$$

where $s_{gw,o}$ represents the specific entropy of the final geothermal water.

3.3 Assessment of the Combined System

After the energetic analysis of the combined system, obtaining the output power and the water production, the definition of total efficiency is proposed with the following expression.

$$\eta_t = \frac{m_w h_{fg} + W_{net}}{m_{gw}(h_{gw,i} - h_{gw,o})} \tag{24}$$

where h_{fg} is the latent heat of the produced water during dehumidification. Furthermore, after obtaining the entropy generation rate for all the involved processes, the total entropy generation rate can be calculated.

$$S_{gen,t} = S_{gen,p} + S_{gen,FE} + S_{gen,tur} + S_{gen,c} + S_{gen,d} + S_{gen,h} + S_{gen,SH} + S_{gen,v} + S_{gen,m} \tag{25}$$

Accordingly, mathematical models of the combined system are built, and then the performance simulation can be executed through the Matlab platform with the established equations.

4. Results and discussion

According to the stream conservation of mass, energy and entropy, the characteristics of power and water combined system driven by geothermal energy is initially simulated, with design conditions shown in Table 1. It can be observed that the mass flow rate and the temperature for the geothermal water is fixed at m_{gw}=3kgs^{-1} and T_{gw}=453.15K, respectively. With respect to the HDH unit, the effectiveness both during the humidification and dehumidification are assumed as ε=0.85, while the seawater sprayed temperature and terminal temperature difference of the seawater heater are assumed at T_{sw2}=353.15K and TTD_{SH}=20K.

4.1 Performance analysis of the flashing power subsystem

In the power and water combined system, the general Rankine cycle with flashing evaporator is first involved. The flashed steam flows into the steam turbine to realize the power generation. Consequently, the specific characteristics of the flashing power subsystem is calculated and presented in Fig. 3. With the increase of the flashing temperature, it is found that the net power, which is calculated as the output power from the turbine minus the power consumption of the geothermal water pump, will first rise to a net power of W_{net}=157.0kW until the flashing temperature arrives at T_{fs}=375.15K. After surmounting the peak value condition, the value of net power declines continuously to W_{net}=96.0kW at the case of T_{fs}=423.15K. Evidently, the net power from the Rankine cycle is determined jointly by the steam mass flow rate and the actual enthalpy drop during the expansion in the turbine. In view of the mass and energy balance within the flashing evaporator, it can be gained that the mass flow rate of the flashed steam will be reduced resulting from the increase of the flashing temperature, from m_{fs}=0.51kgs^{-1} at T_{fs}=363.15K to m_{fs}=0.19kgs^{-1} at T_{fs}=423.15K. Finally, in combination with the continuous increase of the enthalpy drop with the inlet temperature elevation into the steam turbine, a maximum value of the net power is obtained as W_{net}=157.0kW when the flashing temperature stays at T_{fs}=375.15K. Furthermore, in order to guarantee the safety of the steam turbine, the steam quality of the turbine exhaust is also calculated and present in Fig. 3. It can be inferred

that the flashing temperature should be lower than T_{fs}=393.15K, ensuring the quality of the discharged steam, x_e, is higher than 0.88, which is regarded as the lower limit for the turbine safety [22]. Accordingly, the effective mass flow rate varies from m_{fs}=0.51kgs^{-1} at T_{fs}=363.15K to m_{fs}=0.36kgs^{-1} at T_{fs}=393.15K, while the relevant top and bottom net power is W_{net}=157.0kW at T_{fs}=375.15K and W_{net}=147.93kW at T_{fs}=393.15K, respectively.

4.2 Entropy analysis of the HDH desalination subsystem

As demonstrated in the previous literature for the HDH desalination unit [23], the entropy analysis must be first executed to judge the actual feasibility of the thermal conditions. Hence, with the conditions of the maximum net power, the entropy generation for all the components within the combined system are calculated and exhibited in Fig. 4. Thereinto, due to the fixed input conditions for the flashing power subsystem, the entropy generation of the relevant components are also fixed, and the values are $S_{gen,p}$=0.02kWK^{-1}, $S_{gen,FE}$=0.29kWK^{-1}, $S_{gen,tur}$=0.14kWK^{-1} and $S_{gen,c}$=0.11kWK^{-1} for the geothermal water pump, flashing evaporator, turbine and the condenser, respectively. Taking all the values of entropy generation into comparison, it can be obtained that the flashing evaporation has the maximum irreversible loss among all the thermal processes, and the top weight approaches 40.4% when the air mass flow rate stays at m_{da}=0.1kgs^{-1}. Moreover, it is also observed that the negative region of the entropy generation emerges at the component of humidifier, within the range from m_{da}=0.3kgs^{-1} to m_{da}=0.4kgs^{-1}. As a result, the cases with the aforementioned condition is not truly existing to achieve the water production.

4.3 Energetic analysis of the power and water combined system

After the entropy analysis of the HDH desalination subsystem, actually the entire combined system, the corresponding energetic analysis can be accomplished. During the entropy generation calculation, the flashing temperature is fixed at T_{fs}=T_{fw}=375.15K to maximize the power generation. However, the conditions with a top net power can not ensure the maximum performance of the HDH desalination unit. As a result, three values of the flashing temperature with T_{fs}=368.15K, 375.15K and 378.15K are appointed to investigate the specific performance

of the combined system, and the water production capacity with the increasing air mass flow rate is presented in Fig. 5. Taking the thermodynamic performance based on first and second law into consideration, it is found each case has its own impossible conditions, and the produced water will rise with the increase of the flashing temperature. On the basis of the definition of effectiveness and heat capacity ratio (HCR) [24], the top values appears at the balance condition of the dehumidifier, HCR_d=1, with m_w=456.93kgh^{-1}, 635.48kgh^{-1} and 711.85kgh^{-1} for the cases of T_{fw}=368.15K, 375.15K and 378.15K, respectively. Actually, based on the mass and energy equilibrium within the flashing evaporator, the mass flow rate of the remaining water from the bottom will rise with the increase of the flashing temperature. A higher mass flow rates both for the air and seawater are in demand to realize the fixed spraying temperature, T_{sw2}=353.15K, and terminal temperature difference of the seawater heater, TTD_{SH}=20K when the flashing temperature increases. Taking the case of HCR_d=1 for instance, the relevant mass flow rate is elevated from m_{da}=0.96kgs^{-1} and m_{sw}=2.07kgs^{-1} at T_{fw}=368.15K to m_{da}=1.5kgs^{-1} and m_{sw}=3.23kgs^{-1} at T_{fw}=378.15K. Due to an constant value for the humidity difference between the air streams at the inlet and outlet of the humidifier, a higher air mass flow rate also indicates a higher water production.

Different from the water production, the total efficiency of the combined system is jointly determined by the net output power, water production and the energy input of the geothermal water. As stated in Fig. 3, the top value of the net power appears as W_{net}=157.0kW when the flashing temperature reaches T_{fs}=375.15K, and relevant net power are W_{net}=155.79kW and 156.69kW at T_{fs}=368.15K and 378.15K, respectively. In combination with the water production, the variation law of the total efficiency with the increasing air mass flow rate is obtained and presented in Fig. 6. In some extent, the change law of the total efficiency is consistent with that of the water production, because the profit of the combined system mainly comes from the aspect of water production. As a result, the total efficiency will also be elevated after the increase of the flashing temperature. Considering the case with the balance condition of the dehumidifier, HCR_d=1, it is seen that the total efficiency is promoted from η_t=31.88% at

T_{fs}=368.15K to η_t=43.98% at T_{fs}=378.15K. The specific performance of the power and water combined system is listed in Table 2. It can be validated that the efficiency elevation is mainly attributed to the increase of the water production, from m_w=456.93kgh^{-1} to m_w=711.85kgh^{-1}, and the energy input declination, from Q_t=1440.06kW to Q_t=1430.55kW.

4.4 Size determination of the power and water combined system

After the thermodynamic performance is obtained, all the parameters within the power and water combined system are determined. Hence, the areas of the heat and mass transfer devices can be calculated based on the mathematical models from He [25]. Thereinto, the plate heat exchangers (PHE), with the geometric details in Table 3, are applied for the condenser, seawater heater and dehumidifier, while packings are filled into the humidifier, and the area details of the heat and mass transfer devices, under three flashing temperatures and respective balance condition of the dehumidifier, are attained and presented in Table 4. It can be found that the area of the dehumidifier has the dominant weight of all the heat and mass transfer areas. Taking the case of T_{fs}=375.15K for example, the area of the dehumidifier reaches A_d=106m^2, while the total areas are A_t=236.45m^2. Obviously, during the dehumidification process, the heat load is transferred from the hot humid air to the feed seawater, and the relevant coefficient is relatively low due to the participation of air.

4.5 Influences from the critical parameters on the performance of the power and water combined system

A. Spraying temperature

As the previous illustration, potential is existing at the respect of the HDH desalination unit to improve the total efficiency of the combined system. Accordingly, sensitivity analysis from the parameter of spraying temperature, T_{sw2}, is first investigated at the fixed flashing temperature of T_{fs}=375.15K, and the change laws of the water production as well as the total efficiency is exhibited in Fig. 7. Once the flashing temperature is assumed to be changeless, the temperature and mass flow rate of the geothermal water out of the flashing evaporator are also

fixed with T_{fw}=375.15K and m_{fw}=2.55kgs^{-1}. It is found that a decreasing the spraying temperature into the humidifier is beneficial to improve the water producing. The top value of water production is raised with an amplitude of 27.62%, which is Δm_w=154.75kgh^{-1} when the spraying temperature is regulated from T_{sw2}=358.15K to T_{sw2}=348.15K. Actually, once a lower spraying temperature is required, to satisfy the energy balance within the HDH desalination unit, the mass flow rate both for the cycling air and seawater will rise, from m_{da}=0.98kgs^{-1} and m_{sw}=2.36 kgs^{-1} at T_{sw2}=358.15K to m_{da}=1. 8kgs^{-1} and m_{sw}=3.52 kgs^{-1} at T_{sw2}=348.15K. On the other hand, the spraying temperature declination also result in the descent of the humidity difference before and after the humidification process. Finally, the weight of the air mass flow rate to the water production exceeds that from the humidity difference, and a top value of water production, m_w=714.94kgh^{-1}, is obtained at the balance condition of the dehumidifier. Furthermore, at the aspect of the total efficiency, it completely rests with the variation of the water production and the released heat from the geothermal water since the net power is fixed at W_{net}=157kW. Due to the mass flow rate elevation in response to the spraying temperature descent, the total energy input of the combined system will also rise from Q_t=1405.85kW at T_{sw2}=358.15K to Q_t=1461.01kW at T_{sw2}=348.15K. In the light of the different weight from the water production and total energy consumption, a maximum value is calculated as η_t=43.30% at T_{sw2}=348.15K when the balance condition of the dehumidifier arrives. The specific performance of the power and water combined system at different spraying temperatures is listed in Table 5.

B. Terminal temperature difference of the seawater heater

Similar with the case for the spraying temperature, the terminal temperature difference of the seawater heater, TTD_{SH}, is also designated to explore the corresponding influence on the water production and total efficiency at the fixed flashing temperature of T_{fs}=375.15K, shown in Fig. 8. For a surface heat exchanger, it is evident that a lower terminal temperature difference means a better heat transfer performance. As a result, to the requirements of mass and energy balance within the HDH desalination unit, a higher mass flow rate of the air and seawater is necessary

to enhance the heat transfer characteristics of the seawater heater in response to a reduced value of terminal temperature difference. It is gained that the corresponding values for the mass flow rates are m_{da}=1.6kgs^{-1} and m_{sw}=3.43 kgs^{-1} at TTD_{SH}=15K, m_{da}=1.33kgs^{-1} and m_{sw}=2.88 kgs^{-1} at TTD_{SH}=20K and m_{da}=1.08kgs^{-1} and m_{sw}=2.33 kgs^{-1} at TTD_{SH}=25K. As a result, the water production is raised with a magnitude of 46.91% after the regulation of the TTD_{SH} from TTD_{SH}=25K to TTD_{SH}=15K. Moreover, owing to the great elevation of the water production, the final total efficiency is raised from η_t=36.06% to η_t=44.18% although the energy consumption from the geothermal water also rises from Q_t=1379.56kW to Q_t=1487.72kW. The specific performance of the power and water combined system at different terminal temperature differences is listed in Table 6.

4.6 Validation of the power and water combined system

For the sake of ensuring the accuracy of the simulation results from the power and water combined system, the built mathematical models should be compared to the experimental or published data. In view of the novelty of the current coupled system, the flashing Rankine cycle power subsystem and HDH desalination unit are validated respectively. At the aspect of the general flashing Rankine cycle, the current simulation results are compared to the data from the double-flash geothermal power plant [4] based on the inlet parameters of the geothermal water, shown in Table 7. It is found that the maximum deviation arises with 2.9% for the mass flow rate of the flashed steam out of the flashing evaporator. With respect to the HDH desalination unit, the published results from Narayan [23] is prescribed to validate the current performance, shown in Fig. 9. During the comparison, two spraying temperatures with T_{sw2}=353.15K and 363.15K, with the ambient temperature $T_{sw,i}$=308.15K, the effectiveness, ε_h=ε_d=0.92, the relative humidity, RH_1=RH_2=1, are involved. It is found that the maximum deviation of GOR emerges as 2.78% when the mass flow rate ratio are located at m_{sw}/m_{da}=2 with a spraying temperature of 363.15K. The small errors about the two involved subsystems verify the accuracy of the established mathematical models.

5. Conclusions

In the present paper, a novel power and water combined system powered with geothermal water is constituted. The thermodynamic performance of the flashing Rankine power cycle and the HDH desalination unit is simulated and illustrated. Furthermore, the influences from the seawater spraying temperature and the terminal temperature difference of the seawater heater are also discussed. After the simulation and analysis, the concluded results are given as follows:

1. The net power of the flashing Rankine cycle varies with the evaporation temperature. A maximum value of the net power emerges as W_{net}=157.0kW when the flashing temperature stays at T_{fs}=375.15K, with a quality of x_e=89.82% to ensure the safety of the steam turbine.
2. Negative region of the entropy generation exists for the component of humidifier within the combined system, and the flashing evaporation has the maximum irreversible loss among all the involved processes, with a maximal weight of 40.4% at the prescribed range of the air mass flow rate.
3. A higher flashing temperature is effective to raise the water production, and the corresponding top value approach m_w=711.85kgh^{-1} at the case of T_{fw}=378.15K. Due to the dominant weight of the water production to determine the energy conversion situation for the combined system, the maximum value of the total efficiency arrives at η_t=43.98% when the flashing temperature is T_{fw}=378.15K.
4. Due to the mass flow rate elevation to balance the mass and energy, reducing the spraying temperature and terminal temperature difference of the seawater heater can raise the performance of the combined system. The simulation results show that the improve amplitudes for the total efficiency are found with 15.28% and 22.52% in response to the variation difference of ΔT_{sw2}=10K and ΔTTD_{SH}=10K.

Acknowledgements

The authors gratefully acknowledge the financial support by the National Natural Science Foundation of China (Grant No. 51406081) and Hong Kong Scholars Program(Grant No. XJ2017040).

376 **References**

377 [1] Y.L. Nian, W.L. Cheng. Evaluation of geothermal heating from abandoned oil wells. Energy, 142 (2018):
378 592-607.

379 [2] A. Sowizdzal. Geothermal energy resources in Poland-Overview of the current state of knowledge. Renewable
380 and Sustainable Energy Reviews, 82 (2018): 4020-4027.

381 [3] S. Jalilinasrabady, R. Itoi, P. Valdimarsson, G. Saevarsdottir, H. Fujii. 2012. Flash cycle optimization of
382 Sabalan geothermal power plant employing exergy concept. Geothermics, 43 (2012), 75-82.

383 [4] M. Yari. Exergetic analysis of various types of geothermal power plants. Renewable Energy, 35
384 (2010):112-121.

385 [5] J.Y. Wang, J.F. Wang, Y.P. Dai, P. Zhao. Thermodynamic analysis and optimization of a flash-binary
386 geothermal power generation system. Geothermics, 55 (2015): 69-77.

387 [6] Y. Yang, Y.W. Huo, W.K. Xia, X.R. Wang, P. Zhao, Y.P Dai. Construction and preliminary test of a
388 geothermal ORC system using geothermal resource from abandoned oil wells in the Huabei oilfield of China.
389 Energy, 140 (2017): 633-645.

390 [7] T.K. Zheng. Thermal Power Plants. Beijing, China Electric Power Press, 2014.

391 [8] X.J. Yao. Renewable Energy and Power Generation Technology. Beijing, Science Press, 2010.

392 [9] J.F. Wang, Z.Q. Yan, M. Wang, S.L. Ma, Y.P. Dai. Thermodynamic analysis and optimization of an (organic
393 Rankine cycle) ORC using low grade heat source. Energy, 49 (2013): 356-365.

394 [10] R. Bahrampoury, A. Behbahaninia. Thermodynamic optimization and thermo-economic analysis of four
395 double pressure Kalina cycles driven from Kalina cycle system. Energy Conversion and Management, 152
396 (2017): 110-123.

[11] J.F. Hinze, G.F. Nellis, M.H. Anderson. Cost comparison of printed circuit heat exchanger to low cost periodic flow regenerator for use as recuperator in a s-CO2 Brayton cycle. Applied Energy, 208 (2017): 1150-1161.

[12] H.F. Zheng. Solar Energy Desalination Technology. Amsterdam, Netherlands Elsevier, 2017: 447-535.

[13] M. Capocelli, M. Balsamo, A. Lancia, D. Barba. Process analysis of a novel humidification dehumidification adsorption (HDHA) desalination method. Desalination, 429 (2018): 155-166.

[14] B.L.D.O. Campos, A.O.S.D. Costa, E.F.D.C. Junior. Mathematical modeling and sensibility analysis of a solar humidification dehumidification desalination system considering saturated air. Solar Energy, 157 (2017): 321-327.

[15] T. Rajaseenivasan, K. Srithar. Potential of a dual purpose solar collector on humidification dehumidification desalination system. Desalination, 404 (2017): 35-40.

[16] O.K. Siddiqui, M.H. Sharqawy, M.A. Antar, S.M. Zubair, Performance evaluation of variable pressure humidification-dehumidification systems, Desalination, 409 (2017) 171-182.

[17] A.E. Kabeel, M. Abdelgaied, Experimental evaluation of a two-stage indirect solar dryer with reheating coupled with HDH desalination system for remote areas, Desalination, 425 (2018) 22-29.

[18] A.M.I. Mohamed, N.A.S. El-Minshawy. Humidification-dehumidification desalination system driven by geothermal energy. Desalination, 249 (2009): 602-608.

[19] N.A.S. Elminshawy, F.R. Siddiqui, M.F. Addas. Development of an active solar humidification dehumidification desalination system integrated with geothermal energy. Energy Conversion and Management, 126 (2016): 608-621.

[20] M.H. Sharqawy, J.H. Lienhard, S.M. Zubair, Thermophysical properties of seawater: a review of existing correlations and data, Desalination and Water Treatment, 16 (2010): 354-380.

[21] W.D. Shen, Z.M. Jiang, J.G. Tong, Thermodynamics. Beijing, Higher Education Press, 1982.

[22] S.H. Huang. Principles of Steam Turbine. Beijing, China Electric Power Press, 2008.

[23] G.P. Narayan, M.H. Sharqawy, J.H. Lienhard, S.M. Zubair. Thermodynamic analysis of humidification dehumidification desalination cycles. Desalination and Water Treatment, 16 (2010): 339-353.

[24] G.P. Narayan, K.H. Mistry, M.H. Sharqawy, S.M. Zubair, J.H. Lienhard, Energy effectiveness of simultaneous heat and mass exchange devices. Frontiers in Heat Mass Transfer, 023001 (2010): 1-13.

[25] W.F. He, D. Han, W.P. Zhu, C. Jia. Thermo-economic analysis of a water-heated humidification dehumidification desalination system with waste heat recovery. Energy Conversion and Management, 160 (2018): 182-190.

Table 1 Typical thermodynamic parameters of the power and water combined system

m_{gw} (kgs^{-1})	T_{gw} (K)	S (gkg^{-1})	$\varepsilon_{h,d}$	RH_1	RH_2	$T_{sw,0}$ (K)	T_{sw2} (K)	TTD_{SH} (K)	TTD_c (K)	PTD_c(K)	a (m^{2}m^{-3})	H_h (m)
3	453.15	35	0.85	1	0.9	288.15	353.15	20	15	5	157	0.3

Table 2 Specific parameters of the combined system at different flashing temperatures

T_{fs} (K)	m_{da} (kgs^{-1})	m_{sw} (kgs^{-1})	x_e (%)	W_{net} (kW)	m_w (kgh^{-1})	Q_t (kW)	η_t (%)
368.15	0.96	2.07	90.57	155.79	456.93	1440.06	31.88
375.15	1.33	2.88	89.82	157.00	635.48	1432.78	40.39
378.15	1.50	3.23	89.51	156.69	711.85	1430.55	43.98

Table 3 Structure details of the plate type heat exchangers

PHE	δ (mm)	S_p (mm^2)	W(mm)	b (mm)	β(°)
Evaporator	0.45	260460	200	4.4	60
Dehumidifier	0.45	260460	200	4.4	60
Condenser	0.45	260460	200	4.4	60

Table 4 Area dimensions of the heat and mass transfer devices at the balance condition of the dehumidifier

T_{fs} (K)	A_c (m^2)	A_{SH} (m^2)	A_d (m^2)	A_h (m^2)	Q_c (kW)	Q_{SH} (kW)	$Q_{h,d}$ (kW)
368.15	92.82	5.25	76.07	38.94	1073.34	200.35	365.38
375.15	84.58	6.76	106.10	39.01	987.26	277.90	508.13
378.15	81.10	7.63	116.58	39.06	950.48	312.76	569.25

Table 5 Specific parameters of the combined system at different spraying temperatures

T_{sw2} (K)	m_{da} (kgs^{-1})	m_{sw} (kgs^{-1})	x_e (%)	W_{net} (kW)	m_w (kgh^{-1})	Q_t (kW)	η_t (%)
348.15	1.80	3.52	89.82	157.00	714.94	1461.01	43.30
353.15	1.33	2.88	89.82	157.00	635.48	1432.78	40.39
358.15	0.98	2.36	89.82	157.00	560.19	1405.85	37.55

Table 6 Specific parameters of the combined system at different terminal temperature difference of the seawater heater

TTD_{SH} (K)	m_{da} (kgs^{-1})	m_{sw} (kgs^{-1})	x_e (%)	W_{net} (kW)	m_w (kgh^{-1})	Q_t (kW)	η_t (%)
15	1.60	3.43	89.82	157.00	753.72	1487.72	44.18
20	1.33	2.88	89.82	157.00	635.48	1432.78	40.39
25	1.08	2.33	89.82	157.00	513.04	1379.56	36.06

Table 7 Performance comparison of the flashing Rankine cycle between the current system and the double-flash geothermal power plant [4]

	m_{gw} (kgs^{-1})	T_{gw} (K)	p_c (kPa)	T_{fs}/T_{fw} (K)	p_{gw} (kPa)	p_{FE} (kPa)	m_{fs} (kgh^{-1})	h_{fs} ($kJkg^{-1}$)	h_e ($kJkg^{-1}$)
Current	1	503.15	96.4	436.15	2797	666.86	0.15	2760.7	2531
Yari [4]	1	503.15	96.4	436.15	2795	666.5	0.15	2761	2531
Error (%)	/	/	/	/	0.07	0.05	2.9	0.01	0

437

Fig. 1 Specific configuration scheme of the combined system for power and water production driven by geothermal energy

Fig. 2 Temperature profiles and psychrometric chart within the power and water combined system

(a) Condenser

(b) Seawater Heater

(c) Psychrometric chart

Fig. 3 Performance of the flashing Rankine cycle with the increase of the flashing temperature

Fig. 4 Entropy generation distribution of the components for the power and water combined system

Fig. 5 Water production of the power and water combined system with the increasing air mass flow rate at different flashing temperatures

Fig. 6 Total efficiency of the power and water combined system with the increasing air mass flow rate at different flashing temperatures

Fig. 7 Water production of the power and water combined system with the increasing air mass flow rate at different spraying temperatures

Fig. 8 Total efficiency of the power and water combined system with the increasing air mass flow rate at different flashing temperatures

Fig. 9 Comparison of GOR between the current results and the published values from Narayan [23]

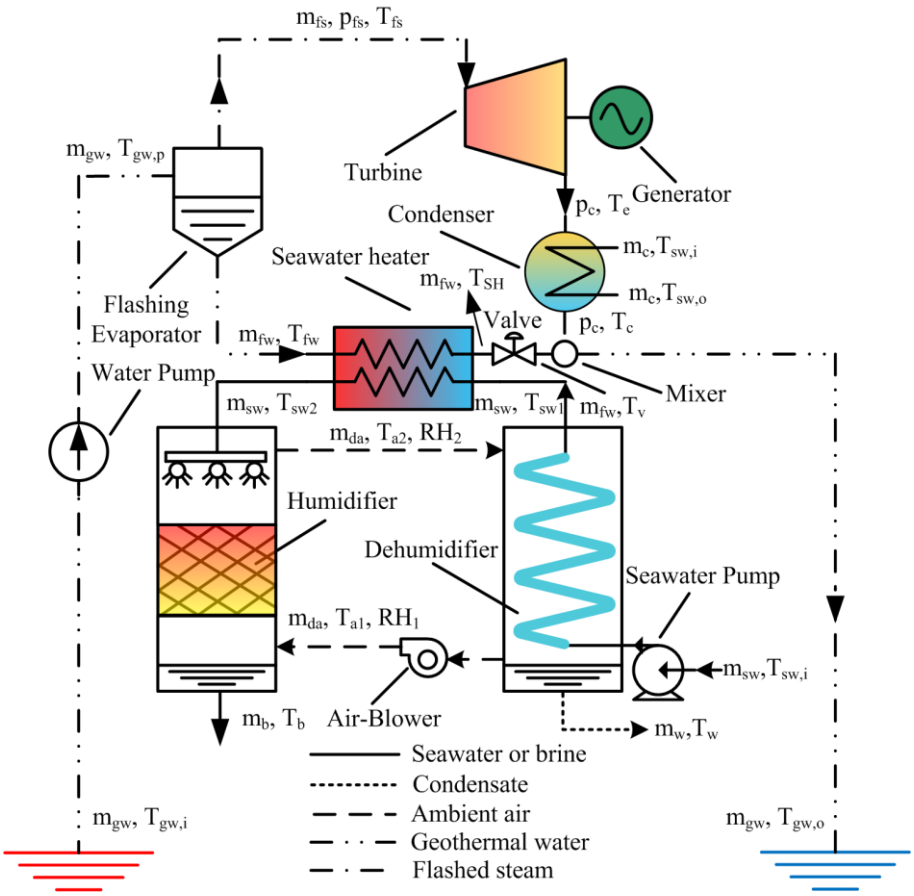

Fig. 1 Specific configuration scheme of the combined system for power and water production driven by geothermal energy

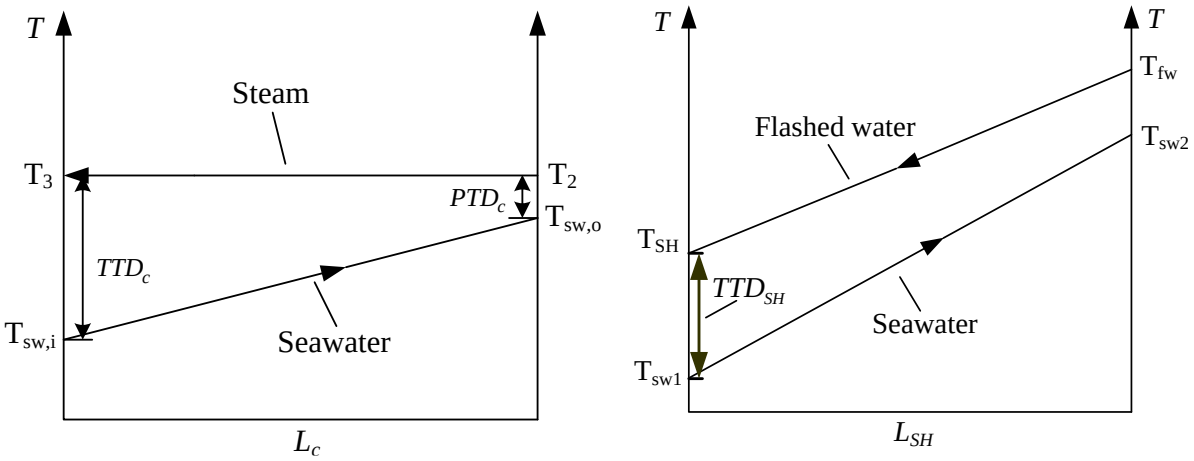

458

459

(a) Condenser

(b) Seawater heater

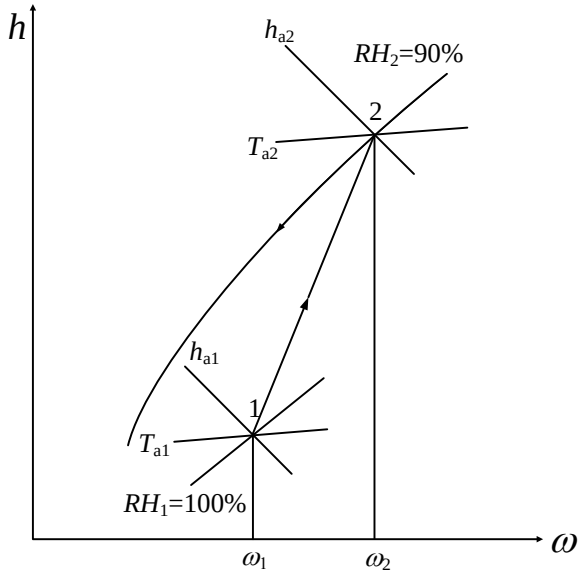

460

461

(c) Psychrometric chart

462 Fig. 2 Temperature profiles and psychrometric chart within the power and water combined system

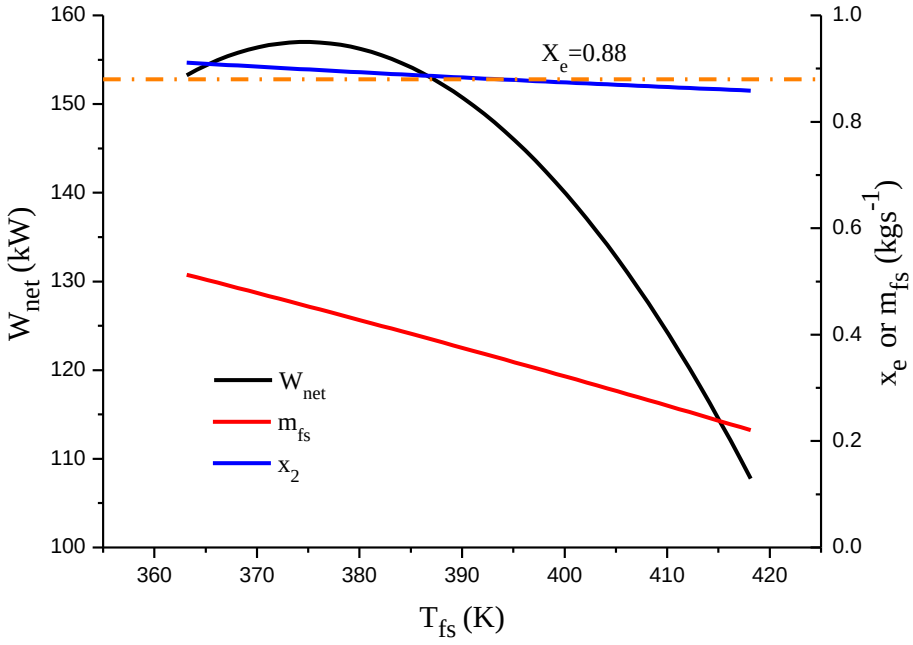

Fig. 3 Performance of the flashing Rankine cycle with the increase of the flashing temperature

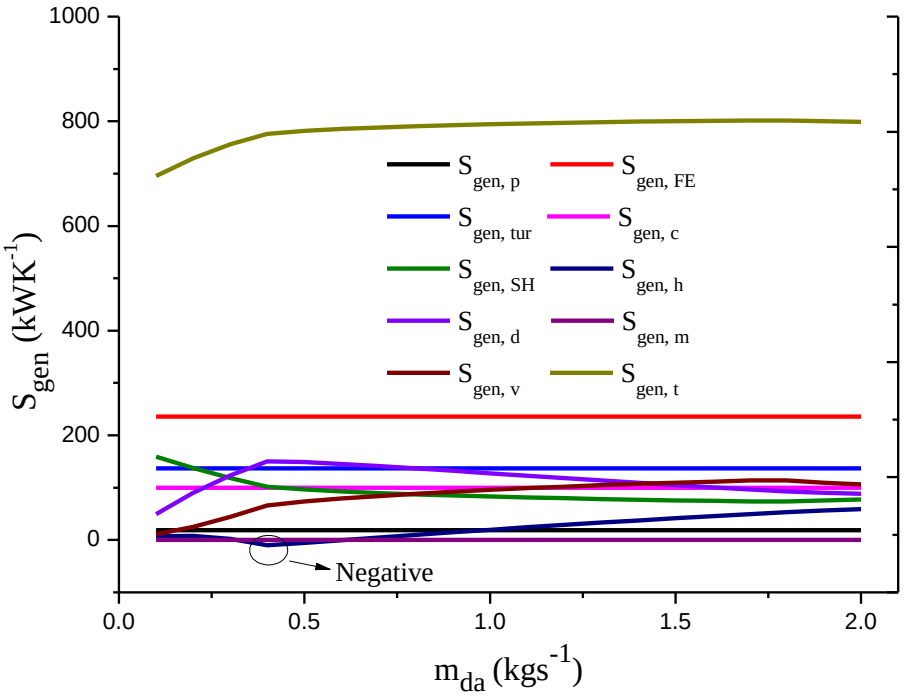

Fig. 4 Entropy generation distribution of the components for the power and water combined system

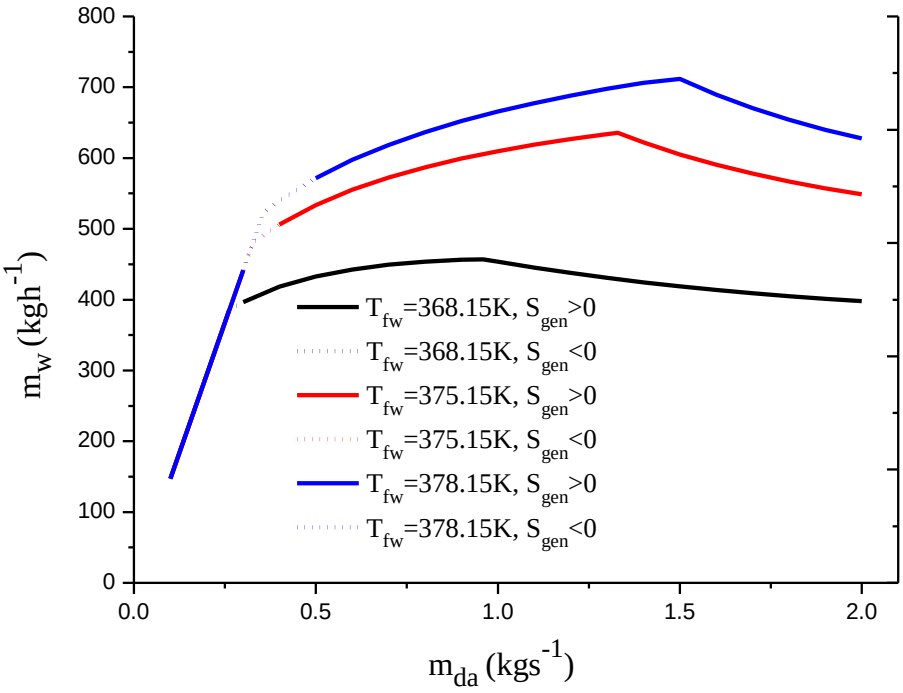

Fig. 5 Water production of the power and water combined system with the increasing air mass flow rate at different flashing temperatures

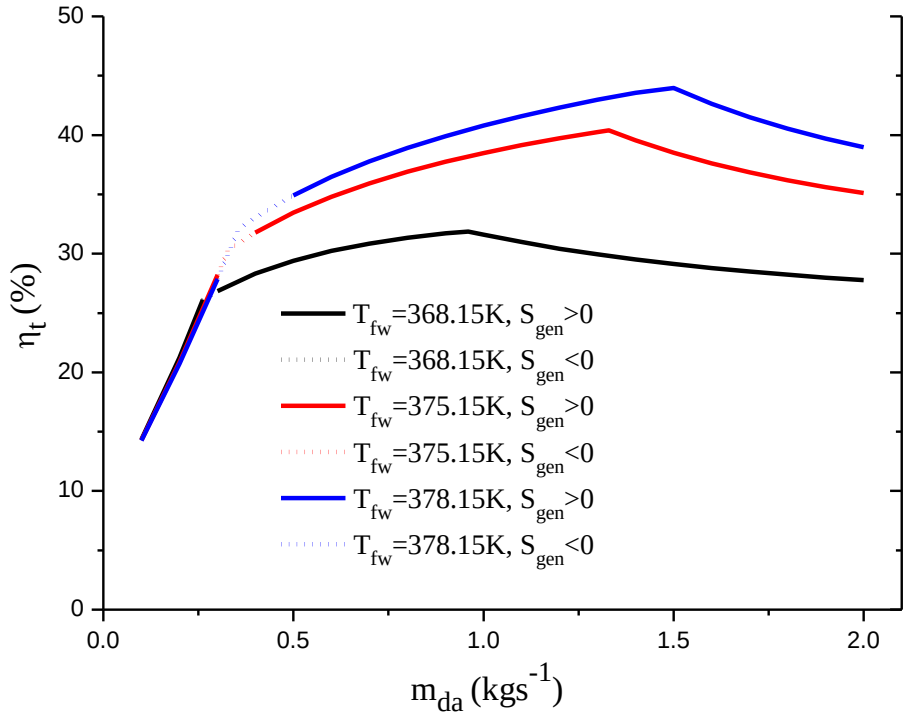

471

472 Fig. 6 Total efficiency of the power and water combined system with the increasing air mass flow rate at different flashing

473 temperatures

474

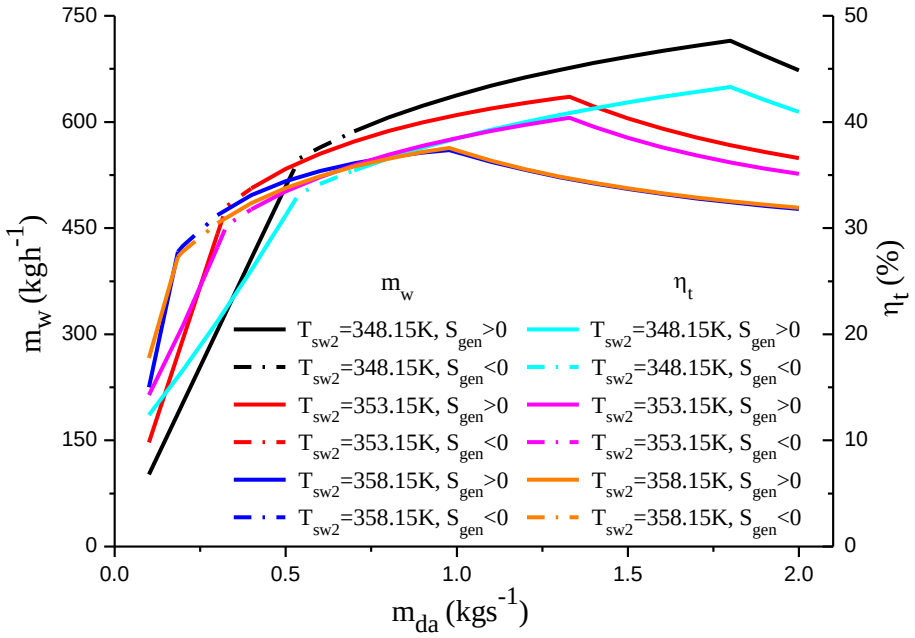

475

476 Fig. 7 Water production of the power and water combined system with the increasing air mass flow rate at different spraying

477 temperatures

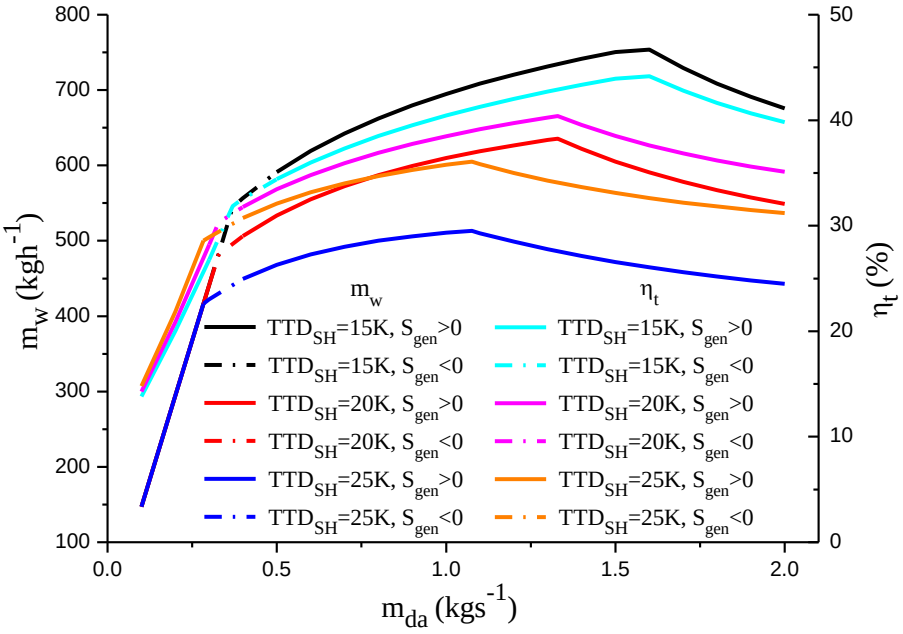

478

479 Fig. 8 Total efficiency of the power and water combined system with the increasing air mass flow rate at different flashing

480 temperatures

481

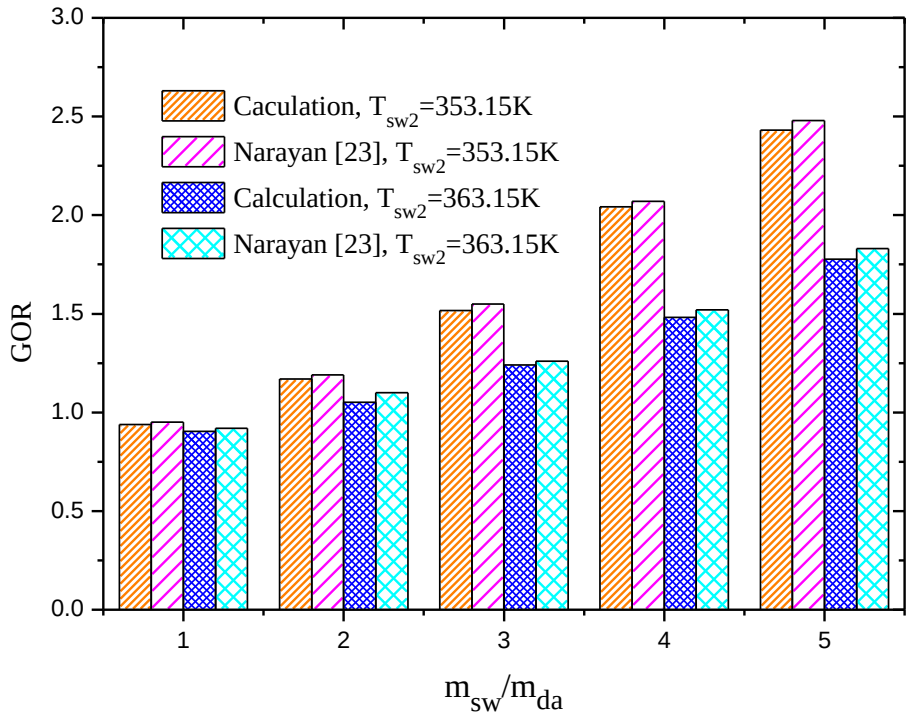

Fig. 9 Comparison of GOR between the current results and the published values from Narayan [23]